Title
What is the importance of climate model bias when projecting the impacts of climate change on land surface processes?

Journal
Biogeosciences, 11(10)

ISSN
1726-4170

Authors
Liu, M
Rajagopalan, K
Chung, SH
et al.

Publication Date
2014-05-16

DOI
10.5194/bg-11-2601-2014

AGU PUBLICATIONS

JGR

Journal of Geophysical Research: Atmospheres

RESEARCH ARTICLE
10.1002/2013JD019784

Special Section:
Nitrogen, Aerosol Composition and Halogens Over a Tall Tower

Key Points:
- Wintertime OH observations
- Significances of HONO as an HO source
- Amplified wintertime oxidation capacity

Correspondence to:
S. Kim,
saewungk@uci.edu

Citation:
Kim, S., et al. (2014), The primary and recycling sources of OH during the NACHTT-2011 campaign: HONO as an important OH primary source in the wintertime, *J. Geophys. Res. Atmos.*, *119*, 6886–6896, doi:10.1002/2013JD019784.

Received 5 MAR 2013
Accepted 25 APR 2014
Accepted article online 30 APR 2014
Published online 10 JUN 2014

The primary and recycling sources of OH during the NACHTT-2011 campaign: HONO as an important OH primary source in the wintertime

Saewung Kim[1,2], Trevor C. VandenBoer[3,4], Cora J. Young[4,5,6], Theran P. Riedel[7], Joel A. Thornton[7], Bob Swarthout[8], Barkley Sive[9], Brian Lerner[5,6], Jessica B. Gilman[5,6], Carsten Warneke[5,6], James M. Roberts[5], Alex Guenther[1], Nicholas L. Wagner[5,6], William P. Dubé[5,6], Eric Williams[5], and Steven S. Brown[5]

[1]Atmospheric Chemistry Division, NCAR Earth System Laboratory, National Center for Atmospheric Research, Boulder, Colorado, USA, [2]Now at Department of Earth System Science, School of Physical Sciences, University of California, Irvine, California, USA, [3]Department of Chemistry, University of Toronto, Toronto, Ontario, Canada, [4]Now at Department of Chemistry, Memorial University of Newfoundland, St. John's, Newfoundland, Canada, [5]NOAA Earth System Research Laboratory, Chemical Sciences Division, Boulder, Colorado, USA, [6]Cooperative Institute for Research in Environmental Sciences, University of Colorado Boulder, Boulder, Colorado, USA, [7]Department of Atmospheric Sciences, University of Washington, Seattle, Washington, USA, [8]Natural Resources and Earth System Science Program, University of New Hampshire, Durham, New Hampshire, USA, [9]Department of Chemistry, Appalachian State University, Boone, North Carolina, USA

Abstract We present OH observations from Nitrogen, Aerosol Composition, and Halogens on a Tall Tower 2011 (NACHTT-11) held at the Boulder Atmospheric Observatory in Weld County, Colorado. Average OH levels at noon were ~ 2.7×10^6 molecules cm^{-3} at 2 m above ground level. Nitrous acid (HONO) photolysis was the dominant OH source (80.4%) during this campaign, while alkene ozonolysis (4.9%) and ozone photolysis (14.7%) were smaller contributions to OH production. To evaluate recycling sources of OH from HO_2 and RO_2, an observationally constrained University of Washington Chemical Mechanism (UWCM) box model (version 2.1) was employed to simulate ambient OH levels over several scenarios. For the base run, not constrained by observed HONO, the model significantly underestimated OH by a factor of 5.3 in the morning (9:00–11:00) and by a factor of 3.2 in the afternoon (13:00–15:00). The results suggest that known chemistry cannot constrain HONO and, subsequently, OH during the observational period. When HONO is constrained in the model by observations (< 50 m), the discrepancy between observation and model simulation improves to a factor of 1.3 in the morning and a factor 1.1 in the afternoon, within the 35% estimated instrumental uncertainty. However, the model produces both a morning and afternoon maximum in OH, in contrast to the observations, which show strong evidence for morning OH production but no distinct morning maximum. Two additional OH sources were also considered, although they do not improve the differences in modeled and measured temporal OH profiles. First, the impact of daytime HONO gradients near the ground surface (< 20 m) was evaluated. Strong HONO gradients were observed between 06:00 and 09:00 MST (mountain standard time), especially within 20 m of the surface. When constrained to HONO observed below 20 m (rather than 50 m), the model produced an even larger morning OH maximum, in contrast to the observations. Second, Cl atoms from $ClNO_2$ photolysis producing RO_2 from reaction with alkanes, while significant, produced steady state Cl atom levels (~ 10^3 atoms cm^{-3}) that were too low to significantly perturb measured OH through reactions of organic peroxy radicals produced from Cl reactions with volatile organic compounds.

1. Introduction

Hydroxyl radicals (OH) maintain the oxidation capacity of the troposphere. The tropospheric OH level is determined by photolytic and recycling sources from the HO_X-RO_X radical pool [*Heard and Pilling*, 2003]. *Levy* [1971] postulated the main OH photolytic production pathway to be initiated by ozone photolysis:

$$O_3 + h\nu\ (< 340\ nm) \rightarrow O_2 + O\ (^1D)\ J_{O3}(O^1D) \quad (1)$$

$$O\ (^1D) + H_2O \rightarrow 2OH\ k_2 \quad (2)$$

where $J_{O3}(O^1D)$ is the ozone photolysis rate to produce $O(^1D)$ and k_2 is the second-order reaction rate constant [e.g., *Sander et al.*, 2011].

Statistical analysis of a long-term OH observation data set (5 years) from rural Southern Germany showed a linear correlation ($r^2 = 0.885$) between OH concentrations and ozone photolysis rates [*Rohrer and Berresheim*, 2006]. The correlation observed was greater than the correlation found between measured and box model calculated OH. Other long-term data sets such as those made in the marine boundary layer by *Vaughan et al.* [2012] have also demonstrated a strong correlation between observed OH and solar radiation.

In spite of these results, solar radiation alone is insufficient to estimate OH levels. Intensive field campaigns that rely on accurate OH for interpretation of photochemical data require deployment of a comprehensive instrumentation suite to constrain photochemical sources of OH [e.g., *Kim et al.*, 2013]. For example, in the correlation plot between ozone photolysis rates and OH concentrations from *Rohrer and Berresheim* [2006], OH concentrations were observed in the wide range of $2–5 \times 10^6$ molecules cm^{-3} for a given $J_{O3}(O^1D)$ value (2×10^{-5} s^{-1}), indicating that OH concentrations depend on multiple variables aside from solar radiation. Furthermore, several recent studies have suggested that the variables governing OH concentrations remain poorly understood. For example, several OH field-observation studies conducted in high isoprene (2-methyl-1,3-butadiene, C_5H_8) environments with moderate to low NO levels (100 parts per trillion (ppt) or less) have reported significant and systematic underestimation of observed OH levels by photochemical box models [*Lelieveld et al.*, 2008; *Hofzumahaus et al.*, 2009]. Although there is current debate regarding OH measurement uncertainty, it has been suggested that such model underestimation is caused by unknown OH recycling sources from peroxy radicals.

Recent research results also suggest uncertainties in constraining photolytic sources of OH. For example, HONO, an important photolytic source for OH (R3), has been observed in higher levels than those that can be explained by our current knowledge of tropospheric chemistry [*VandenBoer et al.*, 2013, and references therein].

$$\mathrm{HONO} + h\nu \rightarrow \mathrm{OH} + \mathrm{NO} \tag{3}$$

This series of recent reports suggests that our current understanding of recycling and photolytic sources of OH is insufficient to constrain OH concentrations in the troposphere. These uncertainties limit the understanding of photochemical ozone and secondary organic aerosol production initiated by OH oxidation of trace gases in the troposphere.

The majority of HO_x field investigations have taken place under summertime and/ or warm conditions characterized by large solar actinic flux and high relative humidity, both of which affect the major photolytic sources for OH. The available OH observations show that our understanding of winter photochemistry is even more limited than it is in summer [*Heard et al.*, 2004; *Ren et al.*, 2006]. *Heard et al.* [2004] reported higher than expected OH levels at noon (1.5×10^6 molecules cm^{-3}) during January and February of 2000 in Birmingham, England. Box model analysis indicated that the dominant OH radical source was ozonolysis of alkene compounds and photolysis of oxygenated volatile organic compounds (VOCs; e.g., formaldehyde). In New York City during the wintertime, *Ren et al.* [2006] reported significantly under-predicted HO_2 by a photochemical box model. However, their modeled OH levels were comparable with the measurements. The dominant primary OH source in New York was HONO photolysis. Different model results with the identical observational data set of *Ren et al.* [2006] come to different conclusions regarding wintertime HO_x, with the analysis of *Cai et al.* [2008] significantly under-predicting measured HO_x.

Here we present observed OH during the NACHTT 2011 (Nitrogen, Aerosol Composition, and Halogens on a Tall Tower) field campaign. This field campaign was conducted at the Boulder Atmospheric Observatory in Weld County, Colorado, USA. Using a comprehensive observational data set [*Brown et al.*, 2013], we evaluate chemical sources and sinks of OH, especially the relative importance of photolytic and recycling sources of OH. We test our understanding of wintertime photochemistry using the University of Washington Chemical Mechanism (UWCM) to determine the influence of ambient HONO and chlorine atom concentrations on the model calculated OH.

The NACHTT campaign included measurements of the major HO_x sources, including photolysis of ozone, HONO [*VandenBoer et al.*, 2013] and $ClNO_2$ [*Thornton et al.*, 2010]. It therefore provides an opportunity to investigate HO_x abundance in an urban/ suburban winter environment concurrently with a unique set of measurements to constrain radical sources during a season when unconventional chemical mechanisms are likely to play an important or even dominant role in oxidant formation.

Table 1. Analytical Measurements Used in the Data Analysis of This Study[a]

Species	Method	Reference or Manufacturer	Sampling Location	Lower Detection Limit
NO, NO_2	CRDS	*Wagner et al.* [2011]	Mobile carriage on tower	~ 20 pptv
$ClNO_2$, Cl_2, N_2O_5	CIMS	*Kercher et al.* [2009]	Mobile carriage on tower	~ 2 pptv
HONO	CIMS	*Roberts et al.* [2010]	Mobile carriage on tower	~ 4 pptv
Speciated VOCs	GC-MS and PTR-MS	*Gilman et al.* [2009] and *de Gouw and Warneke* [2007]	Ground trailer	~ 10 pptv
O_3	UV absorption	Thermo Environmental Instruments 49C	Ground trailer	~ 250 pptv
CO	IR absorption	Thermo Environmental Instruments 48C	Ground trailer	~ 40 ppbv
Photolysis rates (J_{NO2} and $J_{O3}(O^1D)$)	Filter radiometer	Metcon, Inc	Ground trailer	NA

[a]pptv, parts per trillion by volume; NA, not available; CRDS, cavity ring-down spectroscopy; GC-MS, gas chromatography–mass spectrometry; PTR-MS, proton transfer reaction–mass spectrometry.

2. Methods

An overview paper for the NACHTT-11 field campaign [*Brown et al*., 2013] has detailed information on the observation site, the deployed instrumentation, and the sampling strategy. The 3 weeks of the observational campaign (late-February to mid-March) show (1) the nighttime radical reservoir species such as $ClNO_2$ and HONO were consistently observed in nighttime urban air, (2) HONO was concentrated near the surface in nighttime, and (3) C_2-C_5 alkane species composed most of calculated OH reactivity of observed VOC species [*Swarthout et al*., 2013]. A chemical ionization mass spectrometer (CIMS) for OH observation was located in a ground trailer along with the measurement suite for VOCs (proton transfer reaction–mass spectrometry and gas chromatography–mass spectrometry systems) and an ozone analyzer. The OH inlet was located 2 m above ground level (AGL). The tower-borne observation data (vertical profiles of 3 m to 270 m AGL) used for the data analysis in this paper were filtered to include only elevations between 1 and 50 m AGL in the analysis of OH data. The elevator returned to surface level approximately once every 20 min during continuous vertical profiling and was parked at an elevation below 50 m otherwise. Table 1 summarizes analytical details about the instruments and observed parameters presented here.

The HONO quantification technique, deployed for the NACHTT campaign, is described in *VandenBoer et al*. [2013]. The negative-ion proton-transfer chemical ionization mass spectrometer utilized CH_3COO^- to ionize species with a lower gas phase proton affinity than acetic acid. The analytical system was integrated on the tower platform for vertical profile sampling. The nominal sensitivity was ~ 10 Hz ppt^{-1}, and the lower limit of detection is 3.8 ppt (2σ) with 17% observational uncertainty.

2.1. A Chemical Ionization Mass Spectrometer for OH Measurements

Measurements of OH were made with an identical configuration as presented in *Kim et al*. [2013]. Ambient OH was chemically converted to $H_2{}^{34}SO_4$ by injection of excess $^{34}SO_2$, followed by chemical ionization using nitrate ions (NO_3^-, R4) [*Tanner and Eisele*, 1995].

$$NO_3^-HNO_3(H_2O)_n + H_2SO_4 \rightarrow HSO_4^-(HNO_3)_m(H_2O)_p + HNO_3 + (H_2O)_r \quad (4)$$

where $m = 0$ or 1 and n, p, and r are dependent upon water vapor concentrations.

The ion clusters from the above ion-neutral reaction are dissociated in the cluster dissociation chamber then analyzed by a quadrupole-channeltron unit. The instrument background was checked at 1 min intervals by injecting excess propane (99.99% by Matheson TRIGAS, Inc.) to chemically remove OH from the air sample. Calibration was conducted at least 3 times a day as described in *Tanner et al*. [1997], *Mauldin et al*. [2010], and *Petaja et al*. [2012]. Ambient water vapor ([H_2O]), measured by a Vaisala humidity sensor (HMP 60), was photolyzed by 184.9 nm light immediately before the chemical ionization section. The number of photons was mapped by a HAMAMATSU phototube (Model# R5764) certified by the National Institute of Standards and Technology. Using the following equation, the generated number density of OH ([OH]) was calculated.

$$[OH] = \varphi_{184.9nm}\,\sigma_{H2O}[H_2O] \quad (5)$$

where σ_{H2O} is the absorption cross section of H_2O (7.2×10^{-20} cm^2 $photon^{-1}$ at 184.9 nm; *Cantrell et al*. [1997]) and $\varphi_{184.9nm}$ is the photon flux (photon cm^{-2}).

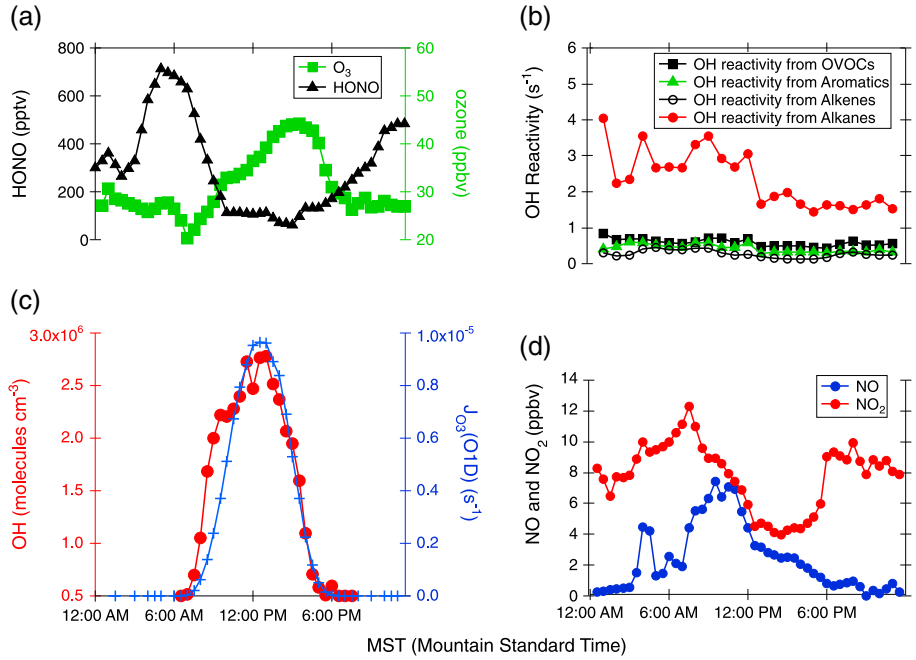

Figure 1. Average diurnal variations of measurements made between 17 February and 28 February 2011 of (a) O_3 and HONO, (b) OH reactivity with different classes of VOCs, (c) OH and $J_{O3}(O^1D)$, and (d) NO and NO_2.

The estimated total uncertainty in OH measured during the NACHTT-11 field campaign is 35%, including statistical errors in the calibration processes (3σ) [*Mauldin et al.*, 2010]. The lower limit of detection is estimated to be 5×10^5 molecules cm^{-3} (2σ) for 10 min integration.

There have been conflicting reports on interferences in OH measurements, especially by the Laser Induced Fluorescence (LIF) technique. The LIF technique for OH quantification has been more widely used than the CIMS technique [e.g., *Heard and Pilling*, 2003]. *Mao et al.* [2012] reported that a conventional background characterization by wavelength modulation with LIF results in measurements of significantly higher (1.5–2.5 times) OH levels compared to those obtained from a chemical removal background method in a forest environment rich in biogenic VOCs. Although measurements during NACHTT were not strongly influenced by biogenic VOCs or their oxidation products, we note that the CIMS-based instruments have commonly used the chemical removal background method. It should be noted, however, that the deployment of the CIMS OH observation technique has mostly been limited to pristine, low biogenic VOC environments such as Mauna Loa Observatory or polar regions [*Heard and Pilling*, 2003; *Mauldin et al.*, 2010; *Liao et al.*, 2011]. In any case, as constraining tropospheric oxidation capacity becomes a crucial research topic to understand regional air pollution and radiative forcers, such as ozone and secondary organic aerosols, respectively [e.g., *Lu et al.*, 2013; *Lelieveld et al.*, 2008], a comprehensive examination of observational and modeling capacity on tropospheric OH should be conducted in many different environments, including the winter season.

2.2. University of Washington Chemical Mechanism

The UWCM 2.1 is equipped with HO_x (= OH + HO_2)-RO_x (organic peroxy and alkoxy radical)-NO_x couplings as described in *Wolfe and Thornton* [2011]. The source code is open to the public and can be downloaded at https://sites.google.com/site/wolfegm/code-archive. Measurements of commonly encountered alkane, aromatic, and alkene species were made by GC-MS and PTR-MS (Table 1). These measured species were extracted from The Master Chemical Mechanism (MCM v3.2; http://mcm.leeds.ac.uk/MCM/ *Jenkin et al.* [2003], *Bloss et al.* [2005], and *Saunders et al.* [2003]) and implemented in the UWCM box model calculations. The chemical mechanisms of 27 VOC species (methane, ethane, propane, *n*-butane, *i*-butane, *n*-pentane, *i*-pentane, neopentane, *n*-hexane, *n*-heptane, *n*-octane, *n*-nonane, *n*-decane, ethene, propene, 1-butene, *c*-2-butene, *t*-3-butene, 1-pentene, *c*-2-pentene, *t*-2-pentene, 2-methyl-1-butene, 2-methyl-2-butene, 1-hexene, *t*-2-hexene, benzene, toluene, and formaldehyde) were incorporated to the UWCM model by including all reactions and intermediate products. These VOCs explained most of the trace gas OH reactivity in the model, as

Table 2. A Summary of Wintertime OH Observations From NACHTT-11 and Previously Published Winter Season Observations[a]

Observed Values at Noon (11 A.M. to 1 P.M., Local Time)	Weld County, Colorado, USA (Late Feb 2011)	New York, New York, USA (January–February 2001)	Birmingham, UK (January–February 2000)
OH (molecules cm^{-3})	~ 2.7×10^6	~ 1.4×10^6	~ 1.7×10^6
$J_{O3}(O^1D)$ (s^{-1})	~ 1×10^{-5}	~ 5×10^{-6}	~ 1×10^{-6}
Ozone photolysis (%)	14.7	1.1	0.6
HONO photolysis (%)	80.4	56.5	36.2
Alkene ozonolysis (%)	4.9	42.4	63.2

[a]The table contains average observed OH concentrations, ozone photolysis rates ($J_{O3}(O^1D)$), and the percentage fractions of primary OH production pathways between 11:00 and 13:00 in local time.

calculated from the observational data set (Figure 1). Measured oxygenated VOCs (OVOCs) contributed insignificant OH reactivity. Formaldehyde (CH_2O) can be an important photolytic source for HO_2 and was constrained by the observed concentrations in the model calculations. Photolysis rates in the model were calculated using the scheme presented in *Saunders et al.* [2003]. We ran the model for 3 days with an identical constraint set to obtain a steady state OH daily variation. The 3 day calculation results are presented below.

3. Results and Discussion

3.1. Observations

The observed daily variations in OH, O_3, $J_{O3}(O^1D)$ HONO, NO_X, and OH reactivity from VOCs during the NACHTT campaign are shown in Figure 1. The noontime (average over 11:30 to 12:30 MST; mountain standard time) OH concentrations were, on average, ~ 2.7×10^6 molecules cm^{-3}. This observed value is higher (by a factor of 1.5 to 1.9) than the concentrations reported from the two previous winter OH observations (Table 2). One may attribute the difference to the fact that $J_{O3}(O^1D)$ during the NACHTT campaign was much higher (2 to 10 times) than the other two winter field campaigns. However, as summarized in Table 2, ozone photolysis was not a major contribution toward OH production for any of the three campaigns compared with the sum of HONO photolysis and alkene ozonolysis. The daily variations in the OH production rate from ozone photolysis, HONO photolysis, and alkene ozonolysis during the NACHTT campaign are shown in Figure 2. HONO photolysis is the dominant primary OH source during the daytime (~ 80% at noon). Alkene ozonolysis was less important to OH production during NACHTT than was observed in previous wintertime field measurements where it was comparable or greater than HONO photolysis. Alkene compounds were observed at typical wintertime U.S. urban background levels [*Gilman et al.*, 2013] and the average OH production rates from ozonolysis of alkenes (11:00–15:00 MST) was 1.1×10^5 molecules cm^{-3} s^{-1}. This average is only 2% of the rate observed in Birmingham from 11:00 to 15:00 MST (5.4×10^6

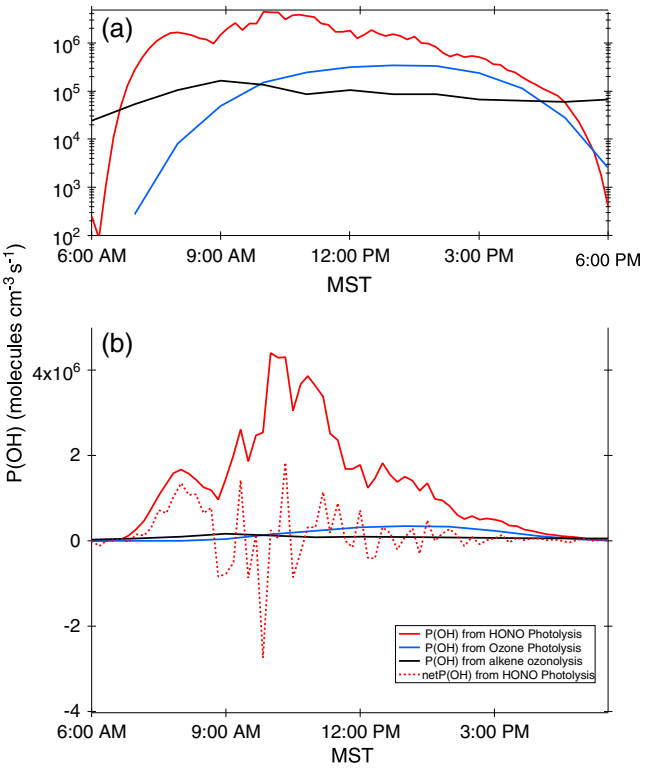

Figure 2. Averaged diurnal variations of primary OH production rates observed during the NACHTT campaign. (a) Note the log-scale on the *y* axis. (b) The net OH production rates.

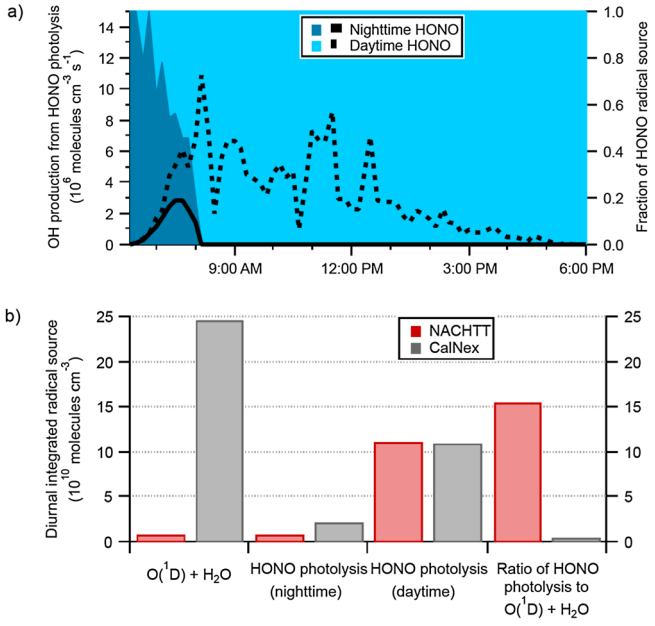

Figure 3. (a) Radical production from photolysis of HONO for both nighttime (before the sunrise 6:20 am MST) and daytime HONO (after the sunrise); (b) Integrated radical production from HONO and reaction of O(^{1}D) with water.

molecules cm^{-3} s^{-1}; *Heard et al.* [2004]). On the other hand, OH production from ozone photolysis (2.9×10^5 molecules cm^{-3} s^{-1}) during the NACHTT campaign was nearly an order of magnitude higher than the rate observed in Birmingham (5×10^4 molecules cm^{-3} s^{-1}). Lastly, the OH production rate from HONO photolysis (3.1×10^6 molecules cm^{-3} s^{-1}) during the NACHTT campaign was the same as the rate observed in Birmingham (3.1×10^6 molecules cm^{-3} s^{-1}). This major contribution of HONO photolysis to OH production is reflected in the observed asymmetrical OH daily variation toward morning (06:00–09:00 MST). When viewed relative to $J_{O3}(O^1D)$, OH concentrations in the morning were higher than those observed in the afternoon, due at least in part to the strong OH production from morning HONO photolysis (Figures 1 and 2) as our subsequent analyses indicate (vide infra).

We can examine this radical source further by distinguishing between the nighttime source of HONO and the variety of proposed, but less certain, daytime sources of HONO (e.g., formation on photoexcited organic substrates [*Ammann et al.*, 1998], from soil pore water [*Su et al.*, 2011], or microbial processes [*Oswald et al.*, 2013]). These daytime HONO processes have not been widely incorporated in tropospheric chemistry modeling studies. Due to its short photochemical lifetime, HONO that is present during daytime, as reported in numerous recent publications, implies a more rapid formation process than the one responsible for its nighttime buildup. Thus, we distinguish daytime production of HONO as chemically distinct from nighttime HONO. These two HONO sources were separated to compare their contribution to the OH formation calculated (Figure 3a). We assume that HONO at, or before, sunrise came solely from nighttime sources such as heterogeneous uptake of NO_2 to ground surfaces or direct emissions and designate it as nighttime HONO. Based on the nighttime HONO levels, the HONO decay after sunrise due to photolysis was calculated, and this loss process was used to estimate the relative contributions of nighttime and daytime HONO to OH production by comparing observed HONO to the calculated nighttime residual HONO as a function of time after sunrise. Radical production from photolysis of HONO was calculated along with the contribution from reaction of O(^{1}D) and water (Figure 3b). All calculations were done using diurnal averages of measurements made below 15 m on clear days while measurements of OH were made (17, 19–26, and 28 February 2011). We assumed that photolysis rate constants vary consistently with time on clear days. Clear days were defined using diurnally integrated J_{NO2} measurements. Only days that had integrated J_{NO2} within 20% of the sunniest day were included.

Nighttime HONO accounted for 7% of the total OH formed from HONO and was important only before 08:30 MST. For the first hour after sunrise, OH formed from nighttime HONO accounted for the majority of the HONO radical source. We compare the OH produced from HONO at NACHTT to another campaign where similar observations and calculations were undertaken. During May and June of 2010, measurements (at 10 m AGL) were made in Pasadena, CA, as part of the CalNex campaign [*Young et al.*, 2012]. In Figure 3b, the diurnal integrated radical production from HONO is compared for both campaigns. It is clear that the magnitude of OH production from HONO is similar in both locations, despite very different environments and conditions. However, if we compare the contribution of the

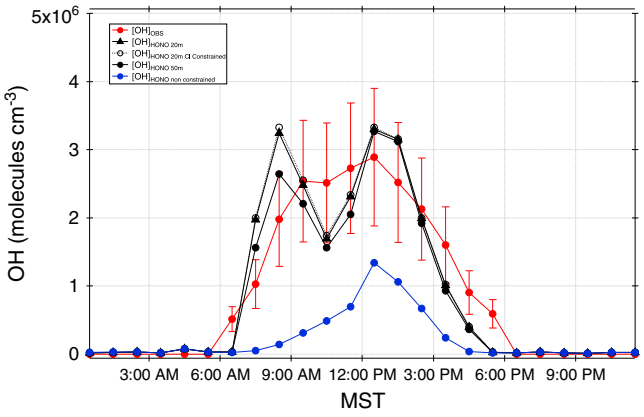

Figure 4. Observed OH daytime variation and the model simulated OH levels for four different model simulation scenarios: (1) observed OH (red), (2)UWCM OH with unconstrained HONO (blue), (3) UWCM OH with constrained HONO averaged HONO between 1 m and 50 m AGL (black solid line with filled circles), (4) averaged between 1 m and 20 m AGL (black solid line with filled triangles), and (5) UWCM OH with constrained HONO and Cl between 1 m and 20 m AGL(black dotted line with unfilled circles).

reaction of $O(^1D)$ with water (R2), we see a dramatic difference between the two campaigns. During CalNex, the dominant radical source was the reaction of $O(^1D)$ with water, which is common for urban summertime conditions [*Alicke et al.*, 2003; *Volkamer et al.*, 2010]. This radical source was approximately twice as important as the contribution from HONO photolysis. In contrast, during the winter conditions of NACHTT, HONO photolysis was the dominant radical source, contributing more than 15 times as many radicals as the reaction of $O(^1D)$ with water.

Lastly, to quantify OH from HONO formed by the termolecular reaction, OH + NO + M, a well-known HONO formation process, the net OH production rates were calculated from equation (6) and are shown in Figure 2b. The data set was filtered for HONO and NO observations below 50 m.

$$\mathrm{netP(OH)_{HONO\ photolysis}} = \mathrm{P(OH)_{HONO\ photolysis}} - \mathrm{L(HONO)_{HONO+OH}} - \mathrm{L(OH)_{OH+NO}} \quad (6)$$

where $L(HONO)_{HONO+OH}$ is a HONO and OH loss term from HONO + OH $\rightarrow H_2O + NO_2$ and $L(OH)_{OH+NO}$ is an OH loss term from OH + NO + M $\rightarrow$ HONO + M.

In the morning (06:00–09:00 MST), the net OH production from HONO ($netP(OH)_{HONO\ photolysis}$) was the dominant OH source. Between 11:00 and 15:00 MST, the net OH contribution from HONO is comparable to or less than ozone photolysis ($netP(OH)_{HONO\ photolysis} = 1.9 \times 10^5$ molecules cm^{-3} s^{-1} versus $P(OH)_{ozone\ photolysis} = 3.2 \times 10^5$ molecules cm^{-3} s^{-1}). For comparison, *Heard et al.* [2004] report winter OH source from HONO photolysis as 6.9×10^5 molecules cm^{-3} s^{-1} in Birmingham, England, in January–February 2000 in the same time period, more than 3 times the net source during NACHTT. However, this is a still significant contribution to OH photolytic production from HONO (~ 37%) during NACHTT because $netP(OH)_{HONO\ photolysis}$ is twice as high as the OH production rate from alkene ozonolysis (9.2×10^4 molecules cm^{-3} s^{-1}).

3.2. Zero-Dimensional Box Modeling Results

The two most important processes maintaining OH levels in the troposphere are primary production and recycling production from peroxy radicals (HO_2) and organic peroxy radicals (RO_2). Henceforth, we will refer to all the direct production pathways of OH from photolytic sources (e.g., ozone and HONO) and alkene ozonolysis as primary sources to differentiate from recycling processes. Since *Levy* [1971] first postulated the importance of tropospheric OH in maintaining oxidation capacity, a reaction between HO_2 and NO has been regarded as the main recycling mechanism for OH. During the NACHTT campaign, alkanes comprised the largest fraction of VOC reactivity to OH among the observed VOC classes by PTR-MS and GC-MS (Figure 1b). Peroxy radical photochemistry from alkane oxidation is relatively well documented [*Atkinson et al.*, 2008], and so it would be expected that box -model calculations constrained by observations will reproduce observed OH levels in this environment. Figure 4 contains the observed OH diurnal variation (red trace) and four different model scenarios described in the caption. In addition, Table 3 summarizes 2 h averaged morning (9:00 to 11:00) and afternoon (13:00 to 15:00) OH concentrations from the observed and model calculated results. The base scenario (blue trace) is a UWCM run that has been observationally constrained as described in section 2.2, excluding HONO observations. The significant underestimation of OH in this model run suggests that gas-phase HONO formation processes included in the UWCM model cannot reproduce the observed HONO levels, resulting in a significantly lower contribution of HONO photolysis to primary OH

Table 3. Comparisons of Observed and Modeled (UWCM) OH Concentrations (Molecules cm^{-3}) in the Morning and Afternoon[a]

	9:00–11:00 (MST)		13:00–15:00 (MST)	
	Concentrations (Molecules cm^{-3})	$[OH]_{OBS}/[OH]_{Model}$	Concentrations (Molecules cm^{-3})	$[OH]_{OBS}/[OH]_{Model}$
$[OH]_{OBS}$	2.6×10^6		2.1×10^6	
$[OH]_{Base}$	4.9×10^5	5.3	6.5×10^5	3.2
$[OH]_{HONO(50m)}$	1.9×10^6	1.3	2.0×10^6	1.1
$[OH]_{HONO(20m)}$	2.2×10^6	1.2	2.0×10^6	1.0
$[OH]_{HONO(20m)+Cl}$	2.2×10^6	1.2	2.1×10^6	1.0

[a]The model was run under five different scenarios with different constraints or scalars applied on observed parameters. We choose 2 h time frames in the morning and the afternoon.

production. A detailed discussion on HONO sources and sinks during the NACHTT campaign can be found in *VandenBoer et al.* [2013]. Simulated OH levels more closely match the observed OH levels when constrained by average measured HONO below 50 m AGL (black trace, Figure 4). The predicted OH, in general, agrees within the observational uncertainty (35%). However, the model results show two [OH] peaks at 7:00 and 13:00 and suppression of OH in between, which was not shown in the observational daily variation.

There are at least two additional factors that likely influence the modeled OH, although neither can reconcile the different temporal profiles of modeled and measured OH. First, *VandenBoer et al.* [2013] observed positive gradients in HONO concentrations near the ground surface, especially during the early morning (06:00–08:00 MST). Measurements of HONO below 50 m AGL were averaged for this work due to the periodic nature of HONO measurements made this close to the surface, as the instrument was investigating vertical profiles up to 250 m AGL on a near-continuous basis. Thus, HONO concentrations at 2 m AGL, where the OH inlet was located, are suspected to be significantly higher than the averaged HONO concentrations from the data set under 50 m AGL, based on the periodic surface level HONO observations, especially if there was a strong surface source of HONO. Such a source could come from surface-deposited HONO during the night, as *VandenBoer et al.* [2013] hypothesized. Indeed, averaged diurnal variations of HONO below 20 m (down to 1 m) and below 50 m AGL (down to 1 m) show positive gradients approaching the ground especially during the early morning (Figure 5).

The higher HONO concentrations observed within 20 m AGL were compared to the previous case and base case. Figure 4 shows that the average HONO measurements below 20 m AGL (black trace, filled triangles), when used as a model constraint enhance OH concentrations, especially in the early morning (20% overestimation, see Table 2 and Figure 4). However, inclusion of this larger morning HONO increases morning OH leading to an even larger estimate of OH near 8:30 than the previous case. This time period (9:00 to 11:00) coincides with the transition between increasing J_{NO2} and decreasing HONO levels (Figure 5). This period has been previously described as a maximum in HONO upward flux from the ground surface [*Ren et al.*, 2011]. If this is also the case during NACHTT, OH concentrations near the surface (e.g., 2 m AGL where the OH instrument inlet was located) could be enhanced in the presence of an upward flux of HONO from the ground surface. Although the larger OH level from HONO photolysis is likely to be more realistic, and eventhough the actual HONO source at 2 m may be larger than the 20 m average, the inclusion of this source does not significantly improve the model to measurement comparison. This is contradictory as the diurnally averaged

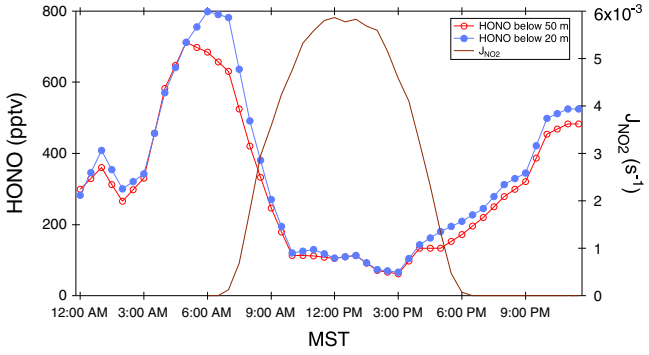

Figure 5. Observed HONO concentrations averaged between 1 m and 50 m (red) and 1 m and 20 m (blue), demonstrating the presence of vertical gradients. The black solid line indicates observed J_{NO2} during the NACHTT campaign.

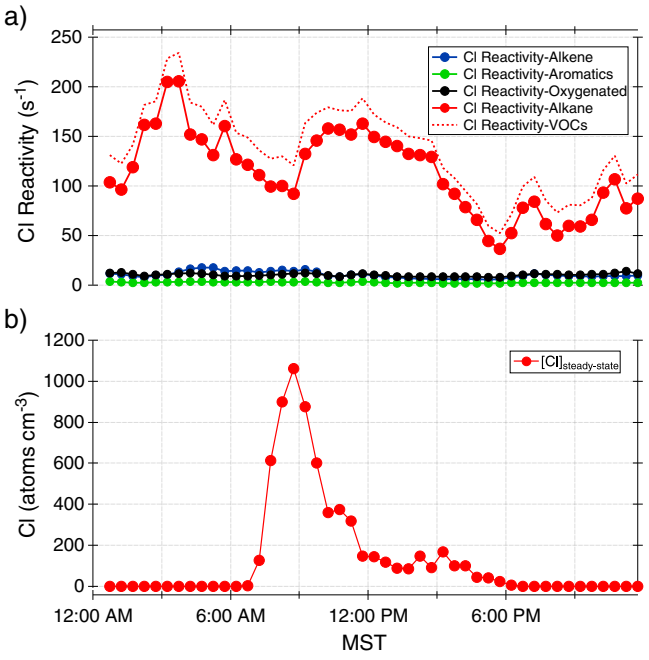

Figure 6. (a) Daily variation of averaged Cl reactivity from total VOCs and (b) estimated $[Cl]_{steady\ state}$.

OH appears to be strongly influenced by a morning source other than ozone photolysis (see Figure 1). The predicted HONO mixing ratio in the base case is below 100 ppt, which is ~3–5 times lower than observed mixing ratios, congruent with the findings of *VandenBoer et al.* [2013] that there is a surface source of HONO during the day at this site. Follow-up studies including vertical gradient measurements of OH near the surface are required to explore the potential role of HONO in maintaining near-surface oxidation capacity during the winter.

The second additional factor influencing radical generation during NACHTT is OH produced via organic peroxy radicals generated from reactions between atomic Cl and alkane compounds. *Thornton et al.* [2010] presented wintertime reactive chlorine observations from February 2009 in Boulder Colorado, which is ~25 km west of the NACHTT field site. Observationally constrained atomic chlorine source estimations indicate a factor of a up to 10 times higher Cl radical production rates than previously estimated values, mostly from the Cl radical reservoir species $ClNO_2$ [*Young et al.*, 2013]. During the NACHTT field campaign, a comparable level of $ClNO_2$ to that reported by *Thornton et al.* [2010] was observed. To estimate Cl atom number densities, we assumed that $ClNO_2$ photolysis was the only Cl atom source and Cl + VOCs as the only Cl atom sink. J_{ClNO2} was estimated from observed J_{NO2} and $J_{O3}(O^1D)$ using the empirical equation (7) developed in *Young et al.* [2012].

$$J_{ClNO2} = J_{NO2} \times (0.03581 \pm 0.00005) + J_{O3}(O^1D) \times (3.70 \pm 0.03) \quad (7)$$

Alkane compounds can explain most of the OH reactivity with the VOCs measured during the NACHTT campaign (Figure 1). Due to fast reaction rates of Cl atoms with alkane compounds, these reactions dominate Cl atom reactivity (Figure 6a). From these observations, we estimated $[Cl]_{steady\ state}$ as

$$J_{ClNO2}[ClNO_2] = k'_{Cl+VOCs}[Cl]_{steady\ state} \quad (8)$$

$$[Cl]_{steady\ state} = J_{ClNO2}[ClNO_2]/k'_{Cl+VOCs} \quad (9)$$

where $k'_{Cl+VOCs}$ is Cl reactivity to VOCs (s^{-1}).

The estimated $[Cl]_{steady\ state}$ is shown in Figure 6b. Estimated number densities of up to 10^3 molecules cm^{-3} are significantly lower than previous estimations of 10^4 to 10^5 molecules cm^{-3} mostly over marine boundary layers [e.g., *Kim et al.*, 2008]. The high levels of alkanes and their rapid reaction with Cl atoms are responsible for the low estimate of $[Cl]_{steady\ state}$. We included the estimated $[Cl]_{steady\ state}$ as a scenario in the model calculations. The low $[Cl]_{steady\ state}$ levels did not increase the modeled OH levels (Figure 4b). Therefore, the potential enhancement in OH production from organic peroxy radicals from alkane + Cl reactions can be ruled negligible.

4. Summary

We presented OH observations collected during the NACHTT campaign at the Boulder Atmospheric Observatory in Weld County, Colorado, in February of 2011. To our knowledge, this study is only the third in depth study of OH in winter. Our observed OH levels are higher than those of two previous studies. HONO photolysis (80.4%), followed by ozone photolysis (14.7%), were found to be the main OH sources during NACHTT. Alkene ozonolysis, reported as a major primary OH source in previous work [e.g., *Heard et al.*, 2004],

was only responsible for ~ 5% of primary OH production during NACHTT. To evaluate recycling sources for OH, we explored observationally constrained UWCM box model simulations. For the base scenario, without constraining observed HONO, the model results significantly underestimate observed OH levels. We found a 3 to 5 times increase in OH concentrations when the model calculation was constrained by the measured HONO ($<$ 50 m). This model calculated OH temporal variation with observed HONO accounts the observed OH temporal variation within the observational uncertainty. However, observed HONO constrained ($<$ 50 m) model calculated OH systematically underpredicted (up to 30%) the measurements, particularly between 9:00 and 11:00. Two possibilities for the higher than expected OH levels in the morning have been discussed: (1) elevated HONO concentrations near the surface originating from HONO vertical gradients near the ground, based on daytime observations; and (2) reaction of Cl atoms with alkanes to produce higher amounts of organic peroxy radicals, a recycling OH source. We found that adopting HONO levels in the model from those averaged over 1–20 m height does not help to reconcile the observed discrepancy. The model calculation actually significantly overpredicted observed HONO especially in the morning. This suggests that the box model scheme does not properly simulate HONO photochemistry especially in the early morning. Steady-state calculations of Cl atom levels produced insufficient excess organic peroxy radicals and also did not appreciably reconcile modeled and observed OH levels. One possible speculation is that the HONO flux from the ground surface source photolyzed to become a significant OH source while elevated HONO was not observed. This is consistent with fine resolution HONO gradient measurements showing increases of roughly a factor of 2 near the ground surface [*VandenBoer et al*., 2013].

Most previous photochemistry observations have been conducted during the summer season. This is understandable because higher temperature and solar radiation regulate photochemical processes to produce secondary photochemical products such as ozone and secondary organic aerosols. This study reports high OH levels that may be attributed to uncertain or poorly characterized HONO sources that have not been fully incorporated in a conventional box model (e.g., UWCM). Although most secondary photochemical pollution problems occur in the summer season, they are also possible in the winter [*Rappengluck et al*., 2013; *Schnell et al*., 2009]. Thus, more thorough investigations of wintertime OH photochemistry should be conducted, especially considering that tropospheric oxidation capacity is an important control on short-lived radiative forcers, such as methane.

Acknowledgments

The National Center for Atmospheric Research is operated by the University Corporation for Atmospheric Research under sponsorship from the National Science Foundation. Any opinions, findings, and conclusions or recommendations expressed in this publication are those of the authors and do not necessarily reflect the views of the National Science Foundation. We thank everyone who helped make NACHTT possible and specifically Gerhard Hübler and Eric Williams for organizing the site logistics and the elevator operation. We acknowledge the use of the Boulder Atmospheric Observatory (BAO), Bruce Bartram of the NOAA/ESRL Physical Sciences Division, and Roya Bahreini of NOAA/ESRL Chemical Sciences Division and CIRES for their help in conducting the measurements at the BAO.

References

Alicke, B., et al. (2003), OH formation by HONO photolysis during the BERLIOZ experiment, *J. Geophys. Res.*, *108*(D4), 8247, doi:10.1029/2001JD000579.

Ammann, M., M. Kalberer, D. T. Jost, L. Tobler, E. Rossler, D. Piguet, H. W. Gaggeler, and U. Baltensperger (1998), Heterogeneous production of nitrous acid on soot in polluted air masses, *Nature*, *395*(6698), 157–160, doi:10.1038/25965.

Atkinson, R., J. Arey, and S. M. Aschmann (2008), Atmospheric chemistry of alkanes: Review and recent developments, *Atmos. Environ.*, *42*, 5859–5871.

Bloss, C., et al. (2005), Development of a detailed chemical mechanism (MCMv3.1) for the atmospheric oxidation of aromatic hydrocarbons, *Atmos. Chem. Phys.*, *5*, 641–664.

Brown, S. S., et al. (2013), The Nitrogen, Aerosol, Composition and Halogens on a Tall Tower experiment, *J. Geophys. Res. Atmos.*, *118*, 8067–8085, doi:10.1002/jgrd.50537.

Cai, C., et al. (2008), Performance evaluation of an air quality forecast modeling system for a summer and winter season – Photochemical oxidants and their precursors, *Atmos. Environ.*, *42*(37), 8585–8599.

Cantrell, C., A. Zimmer, and G. Tyndall (1997), Absorption cross sections for water vapor from 183 to 193 nm, *Geophys. Res. Lett.*, *24*(17), 2195–2198, doi:10.1029/97GL02100.

de Gouw, J., and C. Warneke (2007), Measurements of volatile organic compounds in the Earth's atmosphere using proton-transfer-reaction mass spectrometry, *Mass Spectrom Rev.*, *26*(2), 223–257.

Gilman, J. B., et al. (2009), Measurements of volatile organic compounds during the 2006 TexAQS/GoMACCS campaign: Industrial influences, regional characteristics, and diurnal dependencies of the OH reactivity, *J. Geophys. Res.*, *114*, D00F06, doi:10.1029/2008JD011525.

Gilman, J. B., B. M. Lerner, W. C. Kuster, and J. de Gouw (2013), Source signature of volatile organic compounds from oil and natural gas operations in Northeastern Colorado, *Environ. Sci. Technol.*, *47*(3), 1297–1305.

Heard, D. E., and M. J. Pilling (2003), Measurement of OH and HO_2 in the troposphere, *Chem. Rev.*, *103*(12), 5163–5198.

Heard, D. E., L. J. Carpenter, D. J. Creasey, J. R. Hopkins, J. D. Lee, A. C. Lewis, M. J. Pilling, and P. W. Seakins (2004), High levels of the hydroxyl radical in the winter urban troposphere, *Geophys. Res. Lett.*, *31*, L18112, doi:10.1029/2004GL020544.

Hofzumahaus, A., et al. (2009), Amplified trace gas removal in the troposphere, *Science*, *324*(5935), 1702–1704.

Jenkin, M. E., S. M. Saunders, V. Wagner, and M. J. Pilling (2003), Protocol for the development of the Master Chemical Mechanism, MCM v3 (Part B): Tropospheric degradation of aromatic volatile organic compounds, *Atmos. Chem. Phys.*, *3*, 181–193.

Kercher, J. P., T. P. Riedel, and J. A. Thornton (2009), Chlorine activation by N_2O_5: Simultaneous, in situ detection of ClNO2 and N2O5 by chemical ionization mass spectrometry, *Atmos. Meas. Tech.*, *2*(1), 193–204.

Kim, S., et al. (2008), Airborne measurements of HCl from the marine boundary layer to the lower stratosphere over the North Pacific Ocean during INTEX-B, *Atmos. Chem. Phys. Discuss.*, *8*, 3563–3595.

Kim, S., et al. (2013), Evaluation of HOx sources and recycling using measurement-constrained model calculations in 2-methyl-3-butene-2-ol (MBO) and monoterpene (MT) dominated ecosystem, *Atmos. Chem. Phys.*, *13*, 2031–2044.

Lelieveld, J., et al. (2008), Atmospheric oxidation capacity sustained by a tropical forest, *Nature*, *452*(7188), 737–740.
Levy, H. (1971), Normal atmosphere: Large radical and formaldehyde concentrations predicted, *Science*, *173*(3992), 141–143.
Liao, J., et al. (2011), Observations of hydroxyl and peroxy radicals and the impact of BrO at Summit, Greenland in 2007 and 2008, *Atmos. Chem. Phys.*, *11*(16), 8577–8591.
Lu, K. D., et al. (2013), Missing OH source in a suburban environment near Beijing: Observed and modelled OH and HO_2 concentrations in summer 2006, *Atmos. Chem. Phys.*, *13*(2), 1057–1080.
Mao, J., et al. (2012), Insights into hydroxyl measurements and atmospheric oxidation in a California forest, *Atmos. Chem. Phys.*, *12*(17), 8009–8020.
Mauldin, L., et al. (2010), South Pole Antarctica observations and modeling results: New insights on HO_x radical and sulfur chemistry, *Atmos. Environ.*, *44*, 572–581.
Oswald, R., et al. (2013), HONO Emissions from soil bacteria as a major source of atmospheric reactive nitrogen, *Science*, *341*(6151), 1233–1235.
Petaja, T., et al. (2012), Sulfuric acid and OH concentrations in a boreal forest site, *Atmos. Chem. Phys.*, *9*(19), 7435–7448.
Rappengluck, B., et al. (2013), Strong wintertime ozone events in the Upper Green River Basin, Wyoming, *Atmos. Chem. Phys. Discuss.*, *13*, 17,953–18,005.
Ren, X., et al. (2006), Behaviour of OH and HO_2 in the winter atmosphere in New York City, *Atmos. Environ.*, *40*(Supplement 2), 252–263.
Ren, X., J. E. Sanders, A. Rajendran, R. J. Weber, A. H. Goldstein, S. E. Pusede, E. C. Browne, K. E. Min, and R. C. Cohen (2011), A relaxed eddy accumulation system for measuring vertical fluxes of nitrous acid, *Atmos. Meas. Tech.*, *4*(10), 2093–2103.
Roberts, J. M., et al. (2010), Measurement of HONO, HNCO, and other inorganic acids by negative-ion proton-transfer chemical-ionization mass spectrometry (NI-PT-CIMS): Application to biomass burning emissions, *Atmos. Meas. Tech.*, *3*(4), 981–990.
Rohrer, F., and H. Berresheim (2006), Strong correlation between levels of tropospheric hydroxyl radicals and solar ultraviolet radiation, *Nature*, *442*, 184–187.
Sander, S. P., et al. (2011), Chemical kinetics and photochemical data for use in atmospheric studies, Jet Propulsion Laboratory and California Institute of Technology, Pasadena, CA, *Evaluation Number 17*, *JPL Publication 10–6*.
Saunders, S. M., M. E. Jenkin, R. G. Derwent, and M. J. Pilling (2003), Protocol for the development of the Master Chemical Mechanism, MCM v3 (Part A): Tropospheric degradation of non-aromatic volatile organic compounds, *Atmos. Chem. Phys.*, *3*, 161–180.
Schnell, R. C., S. J. Oltmans, R. R. Neely, M. S. Endres, J. V. Molenar, and A. B. White (2009), Rapid photochemical production of ozone at high concentrations in a rural site during winter, *Nat. Geosci.*, *2*(2), 120–122.
Su, H., Y. F. Cheng, R. Oswald, T. Behrendt, I. Trebs, F. X. Meixner, M. O. Andreae, P. Cheng, Y. Zhang, and U. Poschl (2011), Soil nitrite as a source of atmospheric HONO and OH radicals, *Science*, *333*(6049), 1616–1618.
Swarthout, R. F., R. S. Russo, Y. Zhou, A. H. Hart, and B. C. Sive (2013), Volatile organic compound distributions during the NACHTT campaign at the Boulder Atmospheric Observatory: Influence of urban and natural gas sources, *J. Geophys. Res. Atmos.*, *118*, 10,614–10,637, doi:10.1002/jgrd.50722.
Tanner, D. J., and F. L. Eisele (1995), Present OH measurement limits and associated uncertainties, *J. Geophys. Res.*, *100*(D2), 2883–2892, doi:10.1029/94JD02609.
Tanner, D. J., A. Jefferson, and F. L. Eisele (1997), Selected ion chemical ionization mass spectrometric measurement of OH, *J. Geophys. Res.*, *102*(D5), 6415–6425, doi:10.1029/96JD03919.
Thornton, J. A., et al. (2010), A large atomic chlorine source inferred from mid-continental reactive nitrogen chemistry, *Nature*, *464*(7286), 271–274.
VandenBoer, T., et al. (2013), Understanding the role of the ground surface in HONO vertical structure: High resolution vertical profiles during NACHTT-11, *J. Geophys. Res. Atmos.*, *118*, 10,155–10,171, doi:10.1002/jgrd.50721.
Vaughan, S., et al. (2012), Seasonal observations of OH and HO_2 in the remote tropical marine boundary layer, *Atmos. Chem. Phys.*, *12*, 2149–2172.
Volkamer, R., P. Sheehy, L. T. Molina, and M. J. Molina (2010), Oxidative capacity of the Mexico City atmosphere - Part 1: A radical source perspective, *Atmos. Chem. Phys.*, *10*(14), 6969–6991.
Wagner, N. L., W. P. Dube, R. A. Washenfelder, C. J. Young, I. B. Pollack, T. B. Ryerson, and S. S. Brown (2011), Diode laser-based cavity ring-down instrument for NO_3, N_2O_5, NO, NO_2 and O_3 from aircraft, *Atmos. Meas. Tech.*, *4*(6), 1227–1240.
Wolfe, G. M., and J. A. Thornton (2011), The chemistry of atmosphere-forest exchange (CAFE) model - Part 1: Model description and characterization, *Atmos. Chem. Phys.*, *11*, 77–101.
Young, C. J., et al. (2012), Vertically resolved measurements of nighttime radical reservoirs; in Los Angeles and their contribution to the urban radical budget, *Environ. Sci. Technol.*, *46*(20), 10,965–10,973.
Young, C. J., et al. (2013), Evaluation evidence for Cl sources and oxidation chemistry in a coastal, urban environment, *Atmos. Chem. Phys. Discuss.*, *13*, 13,685–13,720.